JOURNAL OF GEOPHYSICAL RESEARCH, VOL. 99, NO. B7, PAGES 13,941–13,956, JULY 10, 1994

Erosion and tectonics at the margins of continental plateaus

Jeffrey G. Masek, Bryan L. Isacks, Timothy L. Gubbels, and Eric J. Fielding
Institute for the Study of the Continents (INSTOC), Cornell University, Ithaca, New York

Abstract. The topography across the eastern margin of the central Andean plateau north of 18°S (Beni region) bears a strong resemblance to the topography of the southern margin of the Tibetan plateau (Nepal Himalaya), with both regions featuring a steep frontal slope and high peaks at the plateau edge. In contrast, the topography of the eastern margin of the central Andean plateau south of 18°S (Pilcomayo region) tapers toward the foreland more gently and has no line of high peaks at the margin. Both the Himalayan and the Beni regions have been the sites for large amounts of denudation, and in both regions, geologic evidence suggests that erosion has been sufficiently vigorous for the physiographic plateau margin to have retreated toward the plateau interior during the Neogene. We hypothesize that the steep frontal slope and high peaks of the Beni region and Himalayan front largely reflect the high orographic precipitation and high erosion rates occurring in these regions and that the more gentle topography of the semiarid Pilcomayo region reflects a tectonic landform only slightly modified by erosion. We propose that orographic precipitation impinging on a plateau margin will generally tend to drop moisture low on the slope, eroding back the plateau while enhancing or maintaining the steep long-wavelength slope. A numerical model coupling orographic precipitation, erosion, and tectonic uplift demonstrates the plausibility of this hypothesis. The erosional efflux in both the Beni and Nepal Himalaya have been considerable, and simple mass balance calculations for the Himalaya suggest that during the Neogene, the erosional mass efflux has generally outpaced the tectonic mass influx. This contrasts with the apparent prior domination of tectonic influx and may reflect a decrease in the rate of tectonic addition during the same period, and/or increased late Cenozoic erosion rates.

Introduction

Recent years have seen a growing recognition that the Earth's topography represents a dynamic signal of the interaction between tectonics and erosion. The most detailed studies, however, have been confined to relatively narrow mountain belts where the erosional mass efflux has nearly kept pace with the tectonic mass influx [e.g., *Adams*, 1980; *Suppe*, 1981; *Koons*, 1989, 1990]. In contrast to these narrow belts, Tibet and the central Andes represent cases where the total tectonic mass influx appears to have overwhelmed erosion, creating large continental plateaus.

An important aspect of the tectonic-climatic system of these plateaus is that orographic precipitation and high erosion rates are confined to the margins of the plateaus, largely shielding the interiors from denudation. Accordingly, while a large fraction of the tectonic mass influx has contributed to crustal thickening within the plateau and surface uplift, only the margins are subject to large amounts of exhumation [*Koons*, 1990; *Molnar and England*, 1990] (Figure 1). In the case of the Tibetan plateau, this weather edge corresponds to the Himalayan mountain chain, while in the case of the central Andean plateau the weather edge corresponds to the Eastern Cordillera and Subandean foreland fold-thrust belt. These margins are also the sites of active thrusting and the highest modern exhumation rates in the orogens [e.g., *Koons*, 1990; *Beaumont et al.*, 1992; *Isacks*, 1992].

The general tectonic similarities between the Eastern Cordillera and the Himalaya provide the basis for a comparative study of the topography of the two regions. Existing evidence indicates that both the eastern Andean margin and the Himalaya have formed as a result of A-type subduction (continental underthrusting), and both regions are bounded by thin-skinned thrusting within the foreland [*Isacks*, 1988; Roeder, 1988; *Gubbels et al.*, 1993; *Molnar*, 1984; *Dewey et al.*, 1988; *Harrison et al.*, 1992]. In addition, the central Andean plateau displays a pronounced latitudinal gradient in both climate and physiography, making the region a natural laboratory for studying the effects of climate variation on topography.

In this paper we examine the erosional-tectonic system operating at the margins of the central Andean and Tibetan Plateaus. First, we show that the topography of the Nepal Himalaya is strikingly similar to that of the wet, high erosion zone of the margin of the central Andean plateau (Beni region) in northwestern Bolivia. The topography in both areas differs substantially from that of the Pilcomayo region of southern Bolivia, a semiarid area with much lower erosion rates. We hypothesize that the similarities in the topography of the Himalayan and Beni regions, and the differences between these areas and the Pilcomayo region, reflect the high precipitation and erosion occurring at the Himalayan and Beni fronts. The long-wavelength topography may thus be a stronger function of climate than of tectonics.

Copyright 1994 by the American Geophysical Union.

Paper number 94JB00461.
0148-0227/94/94JB-00461$05.00

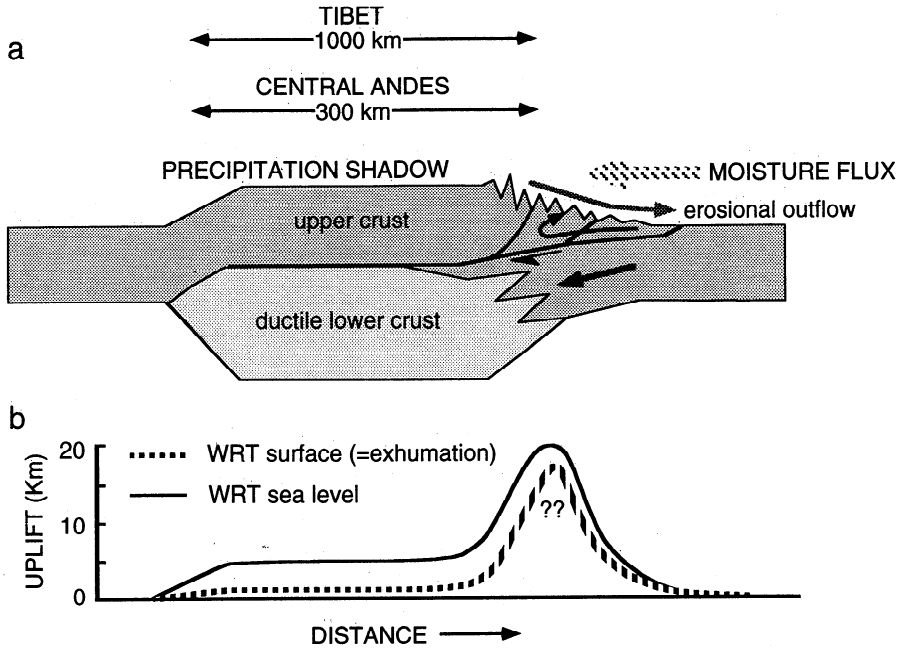

Figure 1. (a) Schematic diagram (not to scale) illustrating climate-tectonic interactions occurring at the margins of continental plateaus. High rates of orographic precipitation and erosion are focused at the margins of the plateau. In contrast, the interior of the plateau is largely shielded from erosion. High local topographic relief is indicative of the active erosion occurring along the windward margin (shown by the jagged line). (b) Uplift curves across the hypothetical plateau shown in Figure 1a [after *Koons*, 1990; *Molnar and England*, 1990]. Uplift of rock with respect to the Earth's surface ('exhumation' or 'denudation') is concentrated at the plateau margin (dashed line). Uplift of the earth's surface with respect to sea level is the net topography and is shown in Figure 1a. Uplift of rock with respect to sea level is defined as the sum of surface uplift and exhumation (solid line). Note that the areas with the highest amount of rock uplift do not correspond to the areas of the highest surface uplift [*Koons*, 1990]. The vertical scale is an approximate lower bound for Tibet, based on available geologic data [*Hubbard et al.*, 1991; *Schelling*, 1992; *Le Pinchon et al.*, 1992].

Second, we present geological evidence suggesting that both the Himalayan and Beni plateau edges have retreated relative to the plateau interiors due to Neogene erosion. This retreat may have been aided by late Neogene shifts in the locus of deformation and possibly by climate change during the late Cenozoic. The interactions of the erosion-tectonic system are illustrated by a simple numerical model illustrating how high orographic precipitation can focus erosion, leading to the steepening and retreat of mountain fronts. We conclude by relating the hypothesized topographic retreat to the total Neogene mass balance for the Andean and Himalayan tectonic wedges.

Observations of Topography and Climate

The two regions of the central Andes referred to in this discussion are the Beni basin and the Pilcomayo basin (Figure 2a). Between 15° and 17°S, within the Beni drainage basin, the Eastern Cordillera is drained by tributaries of the Amazon River. Between 19° and 21°S, within the Pilcomayo drainage basin, the Eastern Cordillera is drained by tributaries of the Parana River. We informally refer to the plateau margins at these latitudes as the Beni region and the Pilcomayo region, respectively. We compare these regions to the Nepal central Himalaya, in the vicinity of the Kathmandu basin (Figure 2b).

The data set is composed of gridded ~5 km resolution topography for the central Andes and ~90 m resolution Defense Mapping Agency (DMA) gridded topography for central Asia [*Fielding et al.*, 1994]. Swath-averaged topographic profiles provide a useful way to characterize the topography of orogenic belts where along-strike variations are small [*Isacks*, 1992]. In this technique a topographic profile is taken perpendicular to strike and all elevations within a specified swath width are projected into the plane of the section. Curves may then be constructed outlining the maximum, minimum, and average elevations within the swath. In areas with little along-strike variation the regional hypsometry is summarized by the curves. For constructional topography with a few isolated peaks the average curve will be close to the minimum, while for recently incised regions with a few major canyons the average curve will be very close to the maximum. The difference between the maximum and minimum envelopes represents a measure of the local relief at length scales of the order of the swath width.

Topographic swaths for the Pilcomayo region, the Beni region, and the Nepal central Himalaya are given in Figure 3, together with precipitation data from World Meterological Organization (WMO) stations [*Hoffmann*, 1979; *Korzoun*, 1977]. There is a clear association between local relief and precipitation at the plateau margins, indicating that local relief is dominantly an erosional signal [*Fielding et al.*, 1994]. Although the annual precipitation budgets for the three regions differ considerably, in all cases the precipitation is orographically controlled, with a maximum in precipitation

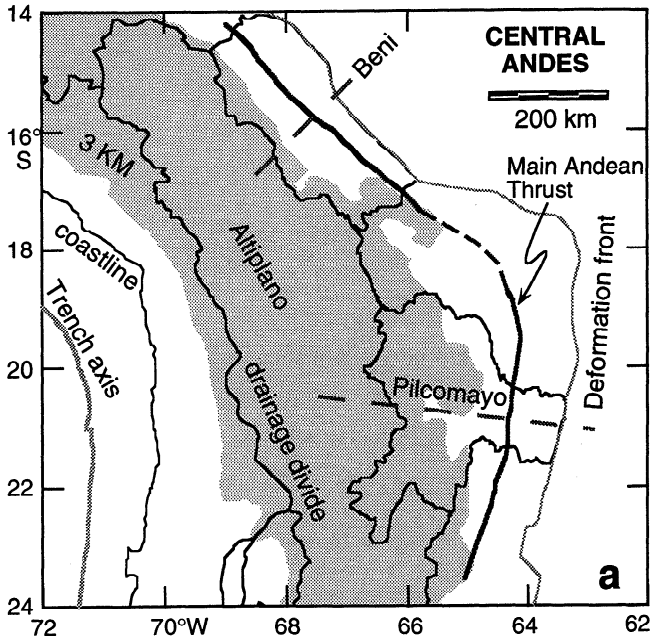

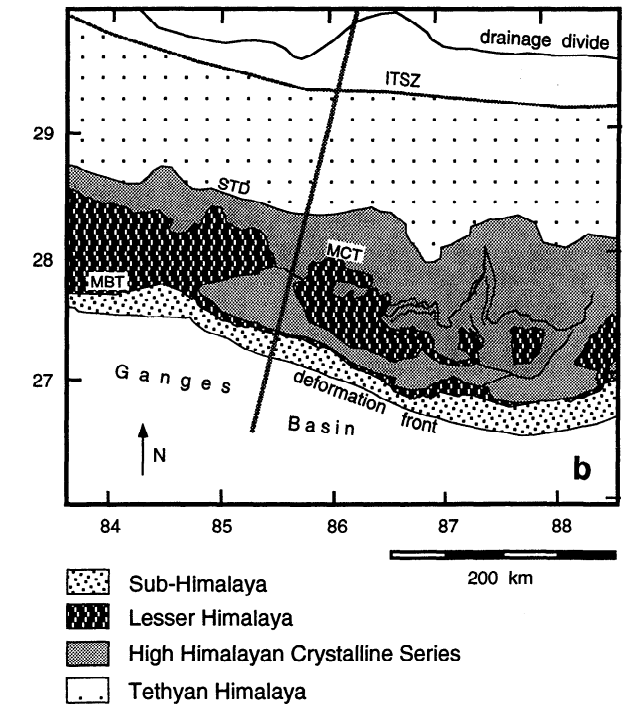

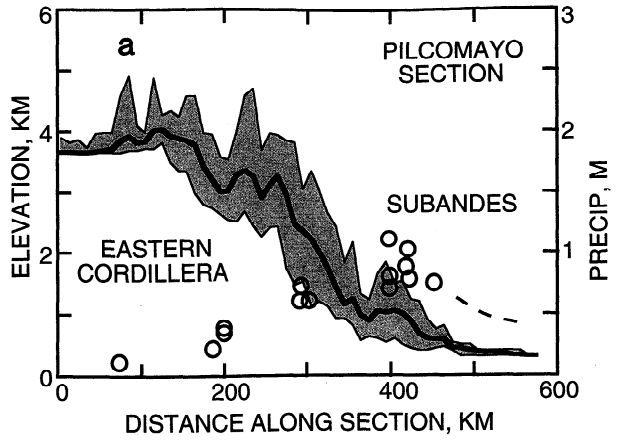

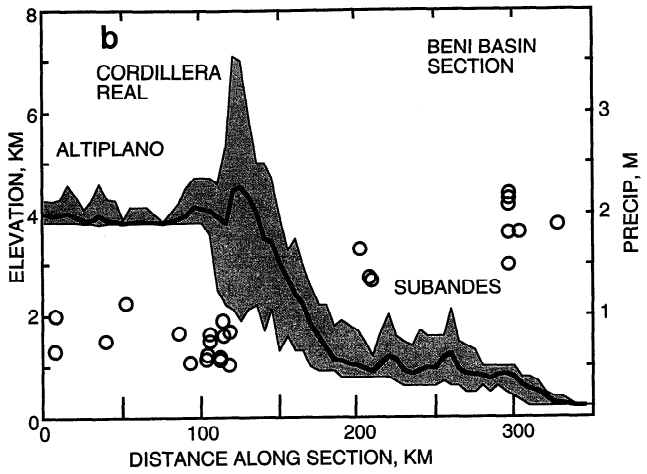

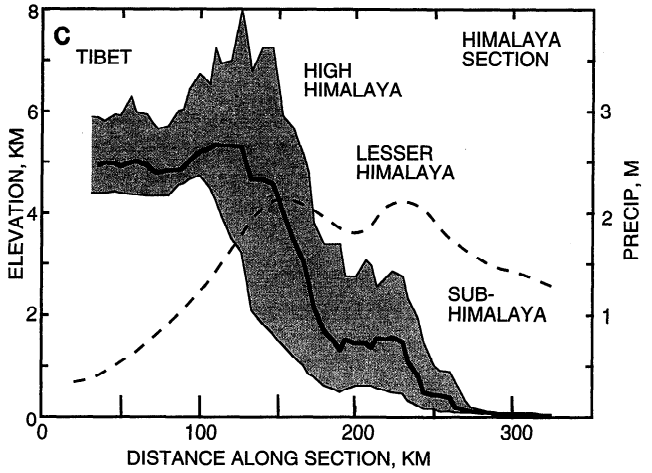

Figure 2. Reference maps for the Central Andes and the Central Himalayan front. Grey lines indicate location of topographic sections displayed in Figures 3 and 5. (a) Central Andean plateau showing deformation front, Main Andean Thrust, and the Beni and Pilcomayo drainage basins. Shaded grey area is above 3 km in elevation. (b) Nepal Himalaya: MBT, Main Boundary Thrust; MCT, Main Central Thrust; STD, South Tibetan Detatchment; ITSZ, Indus-Tsangpo Suture Zone; MS, Mahabharat synclinorium. The position of the STD is approximate and is based on the contact between Tethyan sediments and the Higher Himalayan Crystalline Series as shown by *Gansser* [1964].

Figure 3. Swath averaged profiles of topography and mean annual precipitation across (a) the Pilcomayo front, (b) the Beni front, and (c) the Nepal Himalaya (locations given in Figure 2). The three topographic curves outline the maximum, minimum, and average envelopes for each swath. Topographic swath widths (parallel to strike) are 100 km. The Andean precipitation is plotted by projecting mean annual precipitation values from individual stations using a 200 km swath width. The Himalayan precipitation is taken from contour maps and uses a swath width of 100 km. Note that the horizontal scale for the Pilcomayo section differs by a factor of 2 from the scale of the other two profiles.

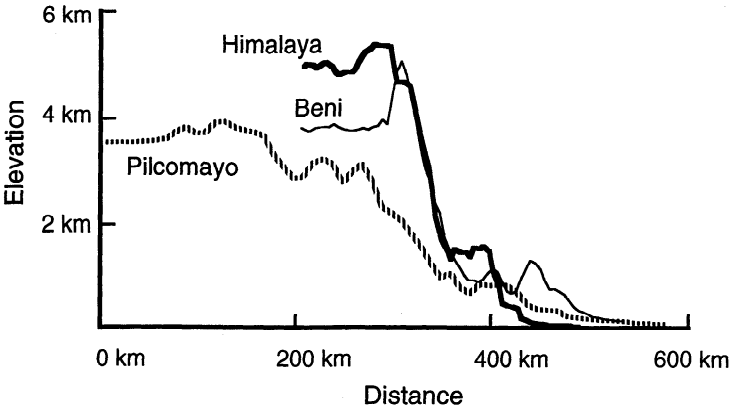

Figure 4. Superposed average elevation curves from Figure 3. Note the similarity between the Himalayan and Beni profiles.

occurring within the foreland or partway up the plateau slope, and not at the highest elevations.

The topography of the central Andean margin shows marked latitudinal variations. In the Pilcomayo region the mean topography of the plateau edge tapers gradually toward the foreland with a regional slope of about 2°. In contrast, the plateau edge in the Beni region shows a very steep falloff immediately to the east of Lake Titicaca, with a regional slope of about 4°. In addition, a line of high peaks (the Cordillera Real) delineates the plateau edge in the Beni region while no such feature is present at the margin of the Pilcomayo region. We also note that the topographic profile for the Central Himalaya at ~85° E bears a strong resemblance to that of the Beni region, with both profiles showing a steep frontal escarpment and a line of high topography (the High Himalaya) at the plateau margin (Figure 4). The major difference between the two profiles is one of scale. The average elevation of the Altiplano plateau is 3.7 km, and the average elevation of the Tibetan plateau is 5.0 km [*Isacks*, 1988; *Fielding et al.*, 1994].

While there exists no evidence for a major change in gross lithology or crustal-scale geometry in the Andes from 16° to 20°S, evidence does exist (discussed in the next section) suggesting that the Beni and Himalayan regions have experienced significantly more denudation than the Pilcomayo region. Accordingly, we hypothesize that the differences between the Pilcomayo profile and the other profiles (Figures 3 and 4) are fundamentally a reflection of erosive power, rather than tectonics.

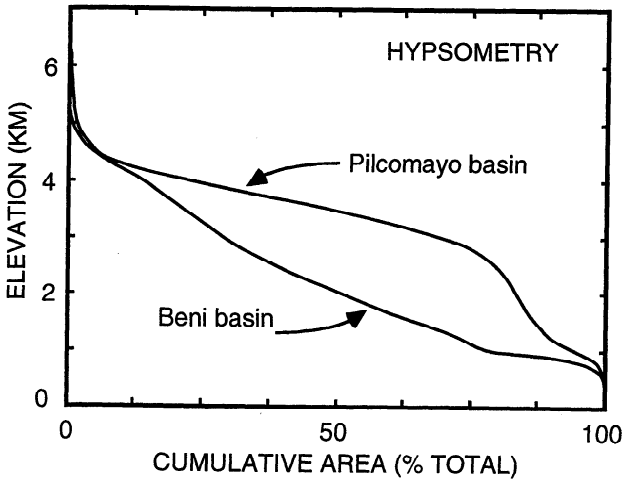

Figure 5. Cumulative hypsometry for the Beni and the Pilcomayo drainage basins. The area under each curve represents the hypsometric integral.

The Beni basin and Central Himalayan front experience monsoonal precipitation amounting to 200-300 cm/yr. In contrast, the Pilcomayo region is semiarid, with the peak precipitation only reaching 70-80 cm/yr, and decreasing markedly up the topographic front (Figure 3). Modern erosion rates calculated from stream gauge data also show greater erosion in the Beni basin compared to the Pilcomayo, by a factor of 2 to 4 [*Guyot et al.* 1988, 1990]. Hypsometric (area-altitude) analysis also suggests that erosion has played a more prominent role in the northern part of Bolivia, with the hypsometric integrals of the northern basins (e.g., Beni) lower than those of the southern (e.g., Pilcomayo) (Figure 5). Following *Strahler* [1952], this may reflect a relative paucity of erosion in the southern basins.

Analysis of an extensive high-level surface preserved as erosional remnants within the Pilcomayo basin suggests the Pilcomayo has experienced relatively little denudation during the late Neogene [*Gubbels et al.*, 1993]. Much of the Eastern Cordillera is covered with ignimbrite sheets stratigraphically correlated with a set of smooth aggradational surface remnants. Dates for these surface remnants cluster about 10 Ma, demonstrating that only minor canyon incision has occured since this time. Furthermore, all deformed strata within the Pilcomayo region of the Eastern Cordillera are unmetamorphosed. Gubbels (1993) concluded from these observations that the vertical denudation over this part of the Andes has amounted to less than 1 km since 10 Ma.

High Neogene Erosion Rates and Plateau Retreat

We have hypothesized that the the present topography of both the Beni region and the Nepal central Himalaya reflects the high precipitation and erosion rates occurring at these margins. A prerequisite for erosionally limited topography is that large amounts of mass be continually denuded from the tectonic uplift pattern. If this efflux were to occur rapidly enough, erosion could outpace thrusting, and the topographic expression of the active margin would tend to retreat toward the plateau interior. This concept is similar to that advanced by *de Paor and Anastasio* [1987], who argued that there is a

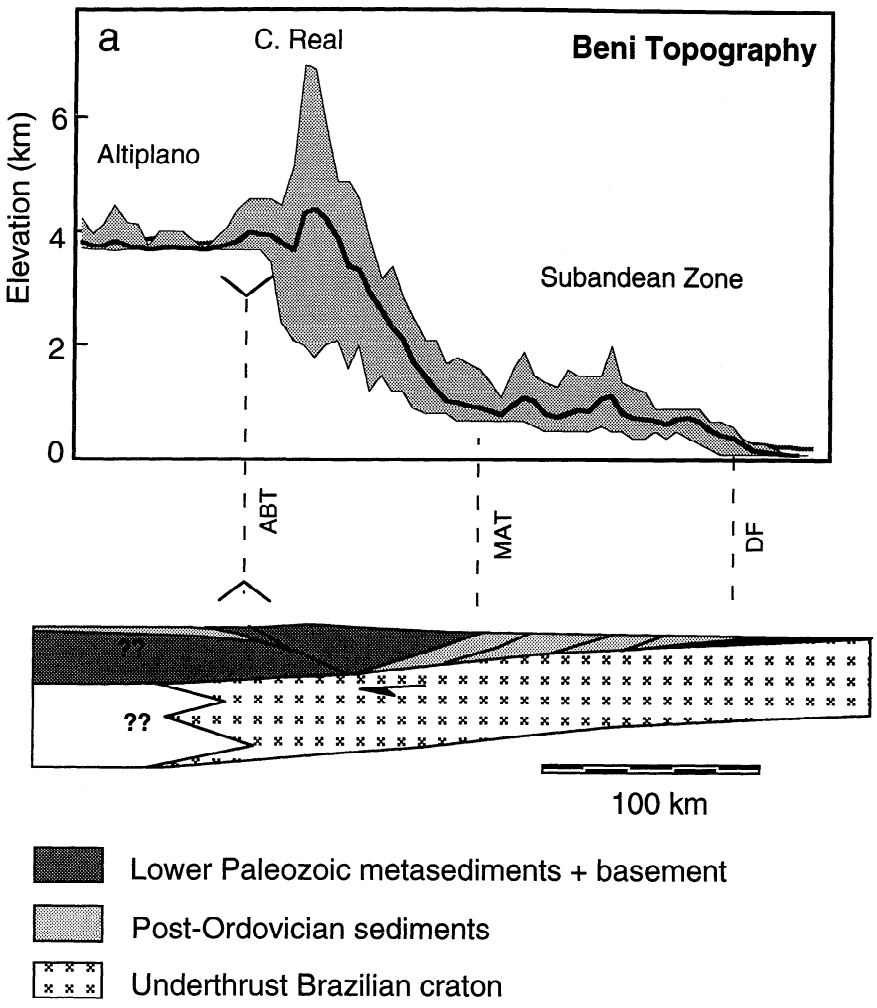

Figure 6a. Overlays of topography and schematic tectonics across the Beni front. The topography is swath averaged (swath width 100 km), with maximum, minimum, and average curves shown. The Andean tectonic section shown is approximately valid for both the Beni and Pilcomayo regions. Correlation of topography with individual strucures is indicated by the dashed line; abbreviations as given in Figure 2.

constant competition between thrust front advance due to slip and thrust front retreat due to erosion. In this section we summarize geologic evidence suggesting that the Beni region and the Himalayan front have been the sites for large amounts of exhumation during the Neogene and that in both regions the plateau margin has retreated relative to the plateau interior during the late Neogene.

Bolivian Andes

The central Andean plateau between 15° and 22°S includes three tectonic elements: the Western Cordillera (magmatic arc), the Altiplano, and the Eastern Cordillera (Figure 2a). The Eastern Cordillera lies along the eastern edge of the plateau and has the gross structural form of a two-sided wedge, thrusting deformed lower Paleozoic rocks over relatively higher structural levels on either side (Figure 6a). The western side of the Eastern Cordillera is bounded by a system of west vergent thrusts that throw lower Paleozoic over Tertiary in many places (Altiplano Backthrust Zone or ABT) [*Roeder*, 1988; *Sempere et al.*, 1990, *Pareja et al.*, 1978]. The eastern side of the Eastern Cordillera is bound by a system of east vergent, crustal-scale thrusts that juxtapose the deformed Paleozoic of the Eastern Cordillera against the folded upper Paleozoic, Mesozoic, and Tertiary of the Subandean fold-thrust belt. This zone of east vergent thrusts includes the Principal Frontal Thrust and Principal Andean Thrust [*Baby et al.*, 1992] and the Main Andean Thrust (MAT) [*Roeder*, 1988] (Figures 2a and 6a).

Several lines of evidence suggest that the Beni region has been a locus for high amounts of exhumation during thc Neogene. The Eastern Cordillera of this region exposes the deepest structural levels found within the Altiplano margin. Although crystalline basement is nowhere exposed from 15° to 22°S, lower Paleozoic strata of the Eastern Cordillera of the Beni region are regionally metamorphosed to staurolite grade [*McBride et al.*, 1987], suggesting at least a few kilometers of denudation. In contrast, there is no evidence for regional metamorphism in the Pilcomayo region. The Eastern Cordillera has been intruded by felsic magmatism along its entire length, with several discrete magmatic episodes punctuating the Mesozoic and Cenozoic [*Evernden et al.*, 1977; *Grant et al.*, 1979]. This magmatism is manifested in

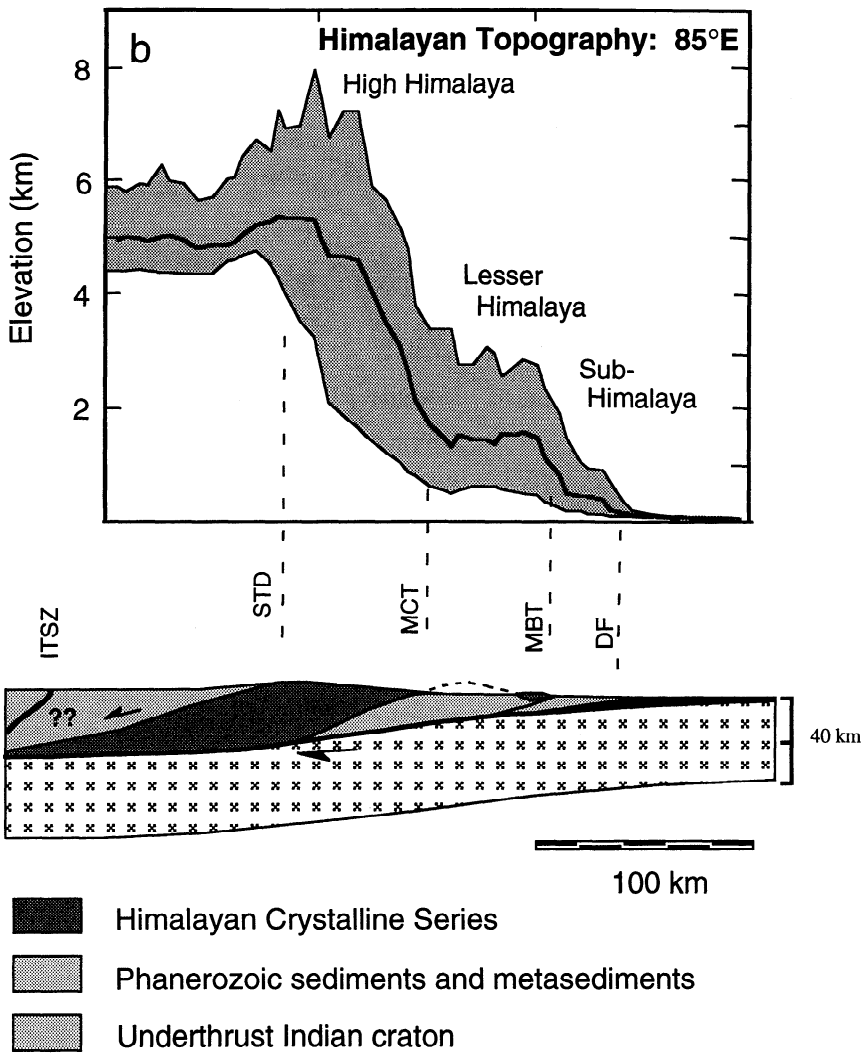

Figure 6b. Same as Figure 6a, except for the central Himalaya at 85°E.

the Pilcomayo region by small isolated subvolcanic intrusive centers, large ignimbrite sheets that overlie Neogene erosional pediments [*Gubbels et al.*, 1993], and the Kari Kari batholith, a resurgent dome within a larger caldera [*Francis et al.*, 1981]. In contrast, the Eastern Cordillera of the Beni region exposes a line of Mesozoic and Cenozoic granitic batholiths which form the high topographic peaks of the Cordillera Real. These granitic intrusions represent relatively deeper structural levels than do the ignimbrites exposed to the south [*McBride et al.*, 1983], again indicating greater denudation in the Beni region.

More quantitative constraints on the amount of Neogene exhumation come from thermochronometric data. *Benjamin et al.* [1987] carried out fission track analyses on apatite and zircon grains from the Zongo and San Gabon granitic plutons and surrounding metasediments within the Eastern Cordillera north of La Paz (Figures 7 and 8b). Although *Benjamin et al.* [1987] compiled the data on a plot suggestive of accelerating denudation during the Cenozoic, the rates used for the last 20 m.y. were derived from the annealing depths and ages of only apatite grains rather than from pairs of apatite and zircon grains [*Benjamin*, 1986]. Thus the calculated exhmation rates were systematically correlated with the ages of the samples. This resulted in a plot of 1/time versus time, necessarily yielding the asymptotically increasing rate curve.

To avoid problems with circularity, we replot the apatite annealing zone to surface transit times from the data of *Benjamin* [1986] against the topography of the Zongo canyon, not against time (Figure 7). Although the annealing temperature of zircon is about twice that of apatite, the zircon grains generally yield annealing dates much older than those of the apatites. Thus, while there is no evidence for steadily accelerating erosion, denudation rates must have been lower prior to 10-15 Ma. Assuming reasonable geothermal gradients for orogenic belts (20-30°C/km) we conclude that approximately 4-8 km of material have been denuded from the upper Beni slope in the past 10-15 m.y. The samples were taken within the Zongo canyon, the topographic profile of which is similar to the minimum topographic profile given on Figure 6a. As the local relief (maximum - minimum) in this area is about 2 km, the 4-8 km of denudation obtained from *Benjamin's* [1986] samples imply about 2-6 km has been denuded from above the maximum topographic envelope in this region.

Additional evidence for large amounts of denudation within the Beni front comes from the analysis of topography. A

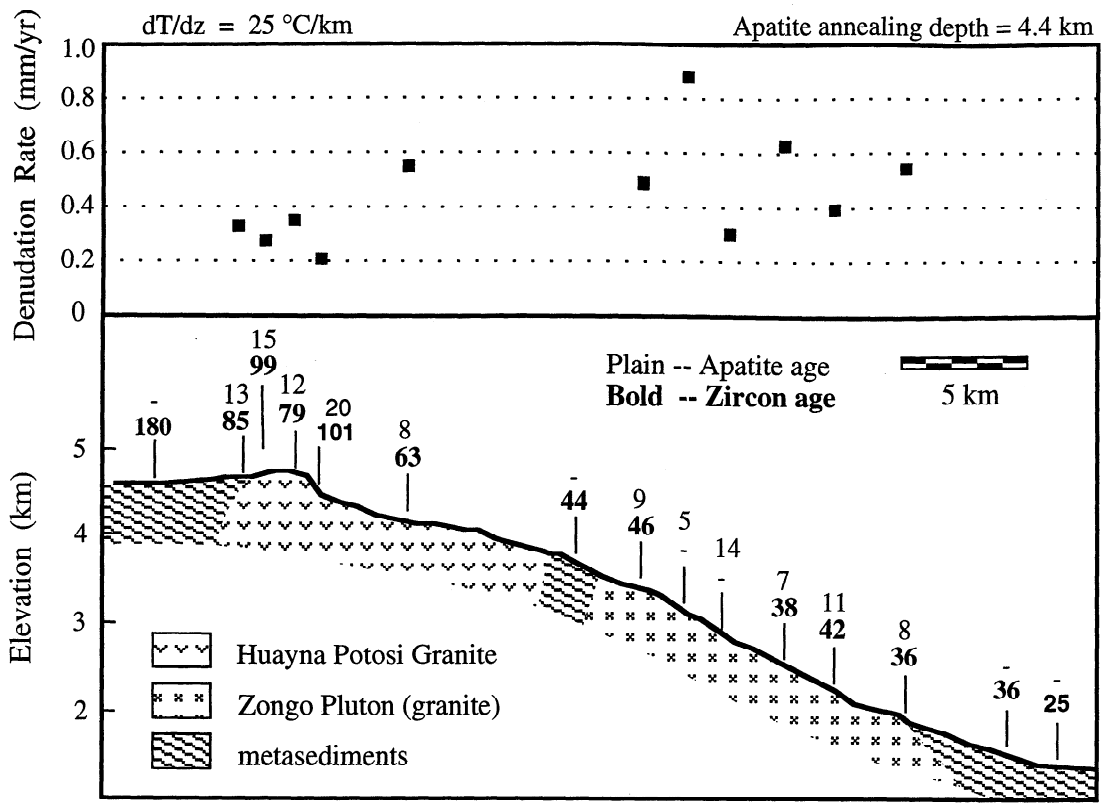

Figure 7. Fission track data from *Benjamin* [1986] plotted against the topography of the Zongo canyon, near La Paz, Bolivia. Topography of Zongo canyon (redrawn from Benjamin, 1986) is shown with sample sites and zircon (lower bold) and apatite (upper plain) annealing ages indicated. Denudation rates are based on apatite ages and an assumed 25°C/km geothermal gradient. Error estimates (2σ) of *Benjamin* [1986] have been omitted but generally lie in the range of 10-30%.

comparison of topography with the main crustal scale structures (Figures 6a and 8) shows that the trace of the Main Andean Thrust does not coincide with the main topographic break but instead lies 20-30 km to the east of the break. This relationship is also indicated on the cross section of *Roeder* [1988]. The simplest explanation for this discrepancy is that the topographic margin of the plateau has retreated back (toward the plateau) from its major bounding structure, the MAT. In contrast, the MAT in the Pilcomayo section (known as the Principal Frontal Thrust) crops out slightly to the west of the main topographic break, suggesting that topographic retreat has been confined to the Beni region.

To summarize, we have provided evidence to suggest that the amount of exhumation in the Beni region been significantly greater than in the Pilcomayo region. In addition, the high erosion rates may have caused the physiographic boundary of the Eastern Cordillera in the Beni region to have retreated westward from its presumed line of origin, relative to the ABT.

Himalaya

The Tibetan plateau has a higher average elevation (~5.0 km) than the central Andean plateau and extends over a much larger area. The Himalaya lie along the southern plateau margin and, like the Eastern Cordillera, are delineated by exposures of relatively deep structural levels, known as the Higher Himalayan crystalline series (Figure 2b). The peaks of the high Himalaya are topographically analogous to the Cordillera Real of the Beni region. Along the northern margin of the high Himalaya, Precambrian gneisses and schists of the crystalline series are placed against Paleozoic and Mesozoic Tethyan sediments and metasediments [*Gansser*, 1964; *Stocklin*, 1980; *Molnar*, 1984]. Unlike the western margin of the Eastern Cordillera, the northern bounding structure, the South Tibetan Detachment [*Burchfiel et al.*, 1992], dips toward the plateau (northward) and has a normal sense of motion (Figures 2b and 6b). To the south, the Main Central Thrust (MCT) separates the High Himalayan crystalline series from predominantly kyanite-grade lower Paleozoic metasediments of the Lesser Himalaya. The Lesser Himalaya are bounded to the south by the Main Boundary Thrust (MBT), and deformation south of the MBT (the Sub-Himalaya) is confined to the Neogene strata of the Ganges foreland basin [*Gansser*, 1964; *Molnar*, 1984].

Unlike the northwestern Bolivian Andes, the major topographic break of the high Himalaya coincides with the principal bounding structure of the plateau, in this case the MCT (Figure 6b). Nevertheless, structural relations within the Nepal Himalaya demonstrate that the Higher Himalayan crystalline series once extended much farther to the south than the present topographic break. In the Nepal Himalaya, the Mahabharat synclinorium extends for several hundred kilometers along strike immediately to the north of the MBT and is composed of kyanite grade crystalline basement (Figures 2b and 6b) [*Gansser*, 1964; *Stocklin*, 1980].

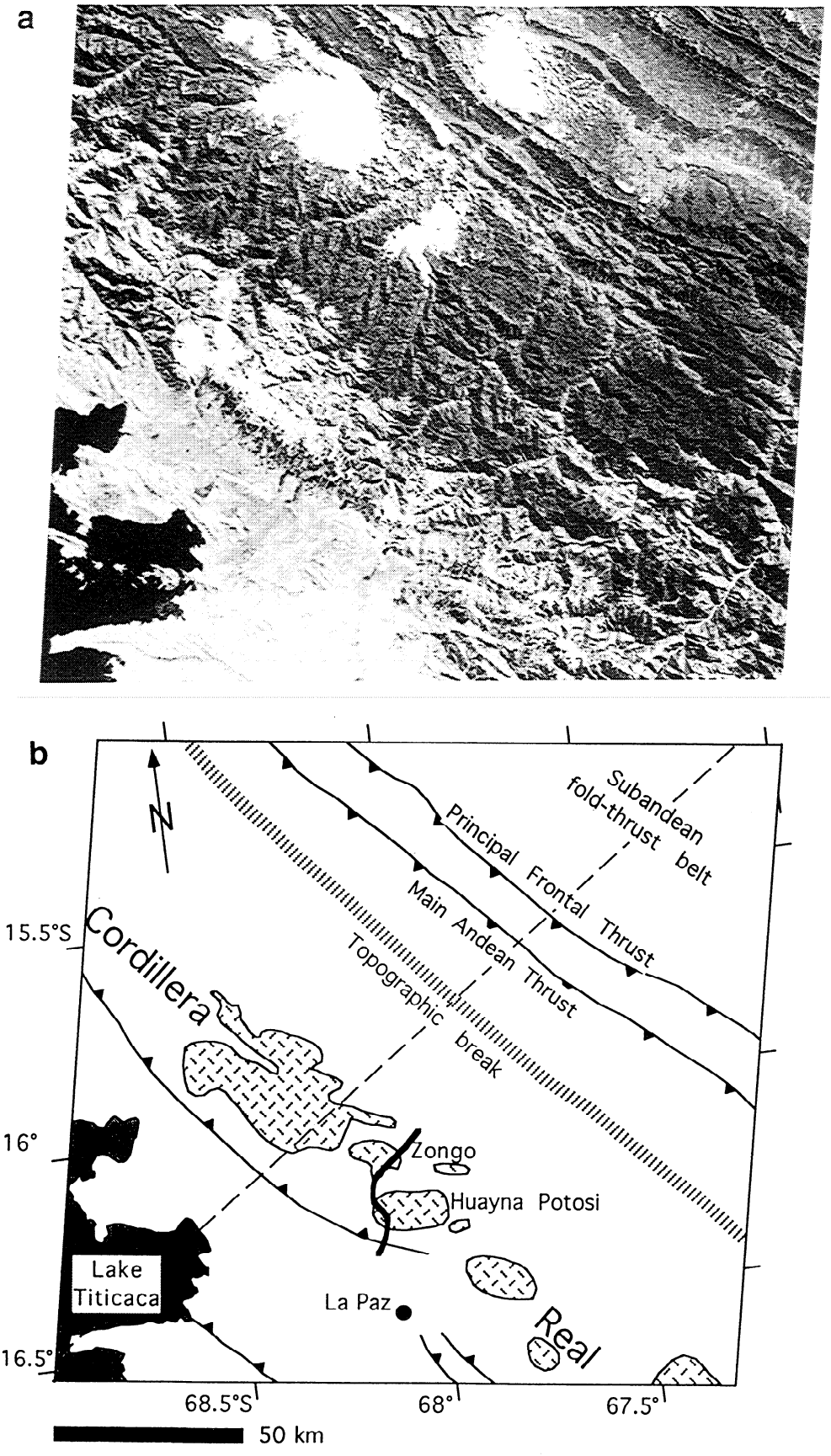

Figure 8. (a) Thematic mapper image for the Beni topographic front northeast of La Paz, Bolivia. (b) Interpretative geologic diagram for the area shown by the satellite image. Note the discrepancy between the outcrop of the Main Andean Thrust and the topographic break (delineated by the abrupt increase shadowed regions of high relief to the west of the MAT). White areas at top of image are clouds. The transect of *Benjamin* [1986] is plotted as the curved bold line through the Cordillera Real.

Structurally, the Mahabharat synclinorium is commonly interpreted as a klippe of the allochthonous MCT thrust sheet overlying the more recently deformed lesser Himalayan metasediments [*Stocklin*, 1980; *Molnar*, 1984; *Schelling*, 1992]. The existence of such a klippe 75 km to the south of the main topographic break and major trace of the MCT demonstrates that at one time the MCT overthrust extended at least to the present trace of the MBT, and possibly farther than that. Insofar as the present high topography of the Himalaya coincideswith the remaining MCT thrust sheet, we conclude that the topographic front of the Himalaya has retreated relative to the STD, similar to the retreat of the Eastern Cordillera in the Beni region.

Thermobarometry from crystalline rocks immediately above the main trace of the MCT indicates that 26±10 km of vertical denudation has occured near the base of the MCT overthrust in Nepal [*Hubbard et al.*, 1991]. Although the crystalline overthrust presumably tapered toward the thrust front, reasonable reconstructions of the MCT overthrust suggest that 10-20 km of material must have been denuded well to the south of the high Himalaya. Although some of this denudation may have been accomplished tectonically through displacement on the South Tibetan Detachment System (STD), the existing geometry of the STD in Nepal [*Burchfiel et al.*, 1992] makes it doubtful that the majority of the denudation of the MCT overthrust could have been accomplished tectonically. The metamorphic grade of the Lesser Himalayan metasediments also attests to substantial heating, presumably during the emplacement of the now eroded overthrust [*Schelling*, 1992].

Timing

A significant observation is that the locus of deformation in both the Bolivian central Andes and the central Himalaya has migrated toward the foreland through time. In the Bolivian Andes, *Gubbels et al.* [1993] dated ignimbrite sheets and Tertiary strata exposed in the Eastern Cordillera between 18° and 22°S and concluded that major compressional deformation of the Eastern Cordillera ceased at approximately 10 Ma. This date marks the earliest possible initiation of Subandean thin-skinned thrusting [*Gubbels et al.*, 1993]. In the case of the Nepal Himalaya, no evidence exists to suggest that the MCT has been active since the earliest Pliocene [*Macfarlane et al.*, 1992], and other authors place the cessation of major activity in the mid-Miocene [*Molnar*, 1984].

It follows that the hypothesized plateau retreat has been occurring on thrust sheets that have been largely inactive since ~5-15 Ma. As in the model of *de Paor and Anastasio* [1987], the topographic retreat of these thrust fronts may have been aided by this inactivity: as slip on the MCT and MAT waned, erosion was able to outstrip the tectonic influx and topographic advance switched to topographic retreat. In the case of the Himalaya, the existence of the Mahabharat synclinorium shows directly that the MCT overthrust advanced toward the foreland and subsequently was eroded back. In the Andes, there is no direct evidence to indicate whether or not a similar pattern of advance and retreat took place, or whether the offset between the MAT and the topographic break has been a steady feature related to the long term balance between thrusting and erosion.

A Numerical Model for Plateau Erosion

The observations presented above indicate that large amounts of material have been denuded from the Beni and Himalayan fronts, both sites of high precipitation and high modern erosion rates. We have also suggested that this erosion has caused both topographic fronts to retreat toward the plateau interiors. We now present a simple numerical model to explain how the erosion of plateau margins can lead to the observed topography of the Beni and Himalayan regions.

General Description

In order to gain insight into the physics underlying the observations given above, we have constructed a simple, process-based numerical model to describe the erosion of uplifting plateau margins. This model is similar in spirit to those presented by *Koons* [1989], *Beaumont et al.* [1992], *Kooi and Beaumont* [this issue], and *Tucker and Slingerland* [this issue].

The model calculates the evolution of a three-dimensional, gridded topographic surface as it uplifts and erodes. The rock uplift due to tectonics is specified as a kinematic function independent of the other model components. This uplift drives a feedback loop composed of simplified models for orographic precipitation, surficial mass transport, and flexural isostasy (Figure 9). Using the synthetic topography at a given time step, we use an orographic algorithm to calculate the spatial distribution of precipitation at each point on the grid. The prevailing wind direction is assumed to be

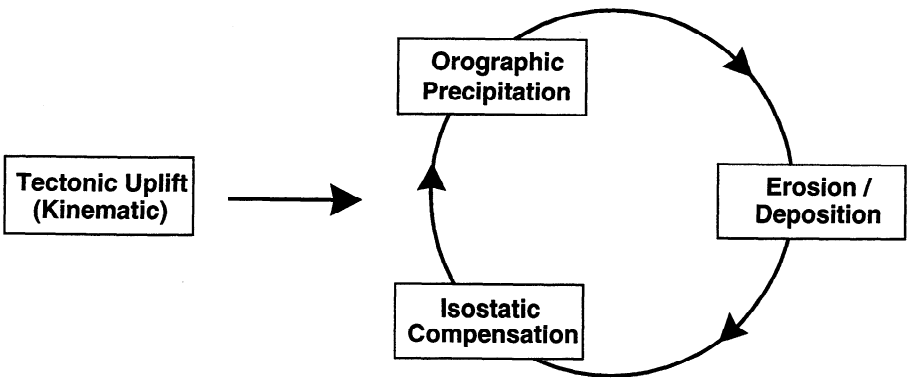

Figure 9. Schematic diagram for the erosional modeling.

perpendicular to strike, impinging on the plateau front. We then use an advective cellular automata erosion/deposition scheme to model surficial mass transport [*Chase*, 1992]. This mass transport is isostatically compensated by the flexure of an infinite elastic plate. The surficial transport and orographic components are discussed in detail in the appendix.

Modeling Results

To validate the orographic algorithm, we have calculated synthetic precipitation distributions for various real and synthetic landforms. We present these results first, then illustrate our uplift function, and finally present results from the coupled erosional model.

Orographic precipitation. The dependence of precipitation on the vertical displacement of an air parcel means that, to a first order, the precipitation rate is slope dependent. To a second order, however, the decrease in the vertical derivative of saturation vapor pressure with increasing height (equation (2), appendix) forces out most of the moisture at lower altitudes. Assuming a saturated incoming air column, the precipitation field given by the model is in reasonable agreement with available data for the Andes and the Himalaya provided by the World Meterological Organization [*Hoffmann*, 1979; *Korzoun*, 1977; *Steinhauser*, 1979]. Figure 10a gives the output of the precipitation algorithm using the average topography of the Altiplano plateau as a lower boundary condition. The output from the model also compares favorably with observed precipitation of regions at higher latitudes, such as the Sierra Nevada of California [*Steinhauser*, 1979] (Figure 10b). In both cases, the algorithm correctly picks the location of maximum rainfall, although it underestimates the precipitation occuring in the lee of the highest topography. To correct this flaw, we have included the option of adding a "background" level of uniformly distributed precipitation in addition to the orographic distribution.

The orographic formulation is roughly appropriate for precipitation due to an air stream being mechanically lifted by a topographic slope, but it is certainly not appropriate for the more difficult problem of precipitation due to local convective instablility. In the latter case, a small topographic pertubation and accompanying release of moisture and latent heat may cause an unstable air parcel to rise catastrophically, resulting in local convective precipitation. It is likely that convective precipitation may account for some part of the precipitation in tropical regions such as the Bolivian Andes and Amazon basin [e.g., *Hastenrath*, 1991]. Nevertheless, the net effect of the convective process is also for moisture to be released low on the slope [*Hastenrath*, 1991], and the lack of a convective parameterization should not affect the general conclusions of this study.

Independent tectonic uplift. The model uses a simple wedge-shaped template for an uplift function. The time evolution of this uplift (Figure 11a) is analogous to that resulting from a crustal scale fault-bend fold [e.g., *Suppe*, 1985], viewed from the reference frame of the hanging wall, combined with an equal uplift within the plateau interior (i.e., left side of Figure 11a). This scenario is conceptually similar to the structural kinematics proposed by *Gubbels* [1993] for the Bolivian Andes and *Zhao and Morgan* [1985] for Tibet. In these models, uplift occurs through crustal-scale thrusting at the plateau margins and ductile lower crustal shortening within the plateau interiors.

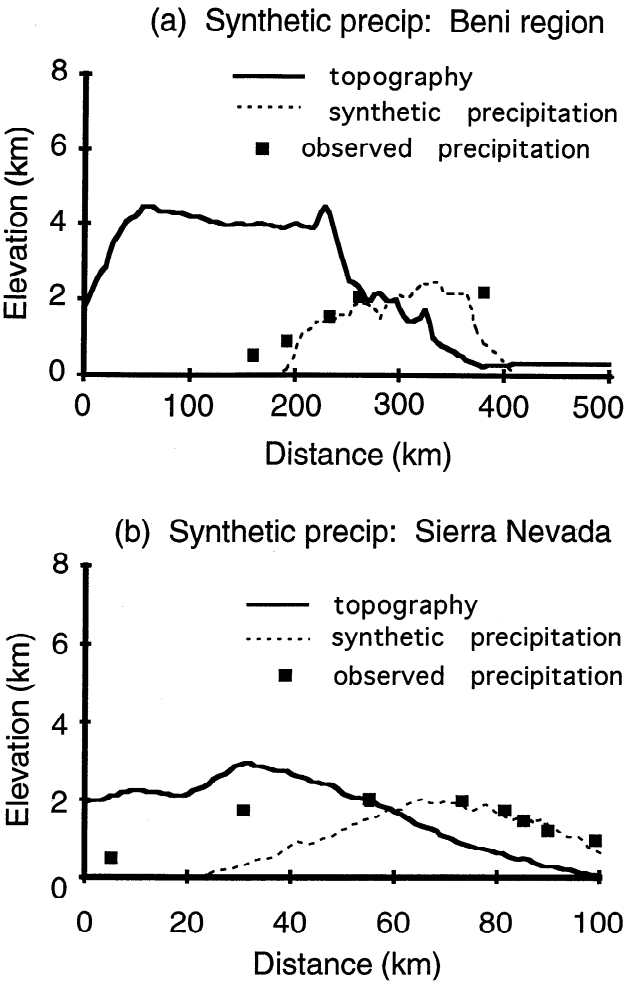

Figure 10. Output of precipitation algorithm run on actual topography for (a) the Altiplano plateau, latitude 16°S and (b) the Sierra Nevada of California. Calculated precipitation (dotted line) and observed precipitation from WMO data (solid circles) are plotted against average topography (solid line). The incoming air column was assumed to be 100% saturated. Since the model only predicts the spatial distribution of precipitation, and not amounts, the amplitude of the precipitation curves have been normalized and no scale is given.

The uplift pattern in Figure 11a is assumed to be isostatically compensated. All further mass transfer due to erosion and deposition is isostatically compensated by the flexure of a three-dimensional, infinite elastic plate [e.g., *Turcotte and Schubert*, 1982]. We use a flexural rigidity of $D = 5 \times 10^{22}$ N m. Although this rigidity is relatively low, it represents a transitional value from the stronger foreland to the weak, ductile interior of the plateau and is consistent with estimates given for the hinterland of the Bolivian Andes by *Lyon-Caen et al.* [1985] and for the high Himalaya by *Lyon-Caen and Molnar* [1983, 1985].

Erosional model. The erosional modeling results are presented in Figures 11b, 11c, and 11d as a series of swath-averaged profiles giving minimum, maximum, and average elevation profiles after 750,000 storm events. The initial

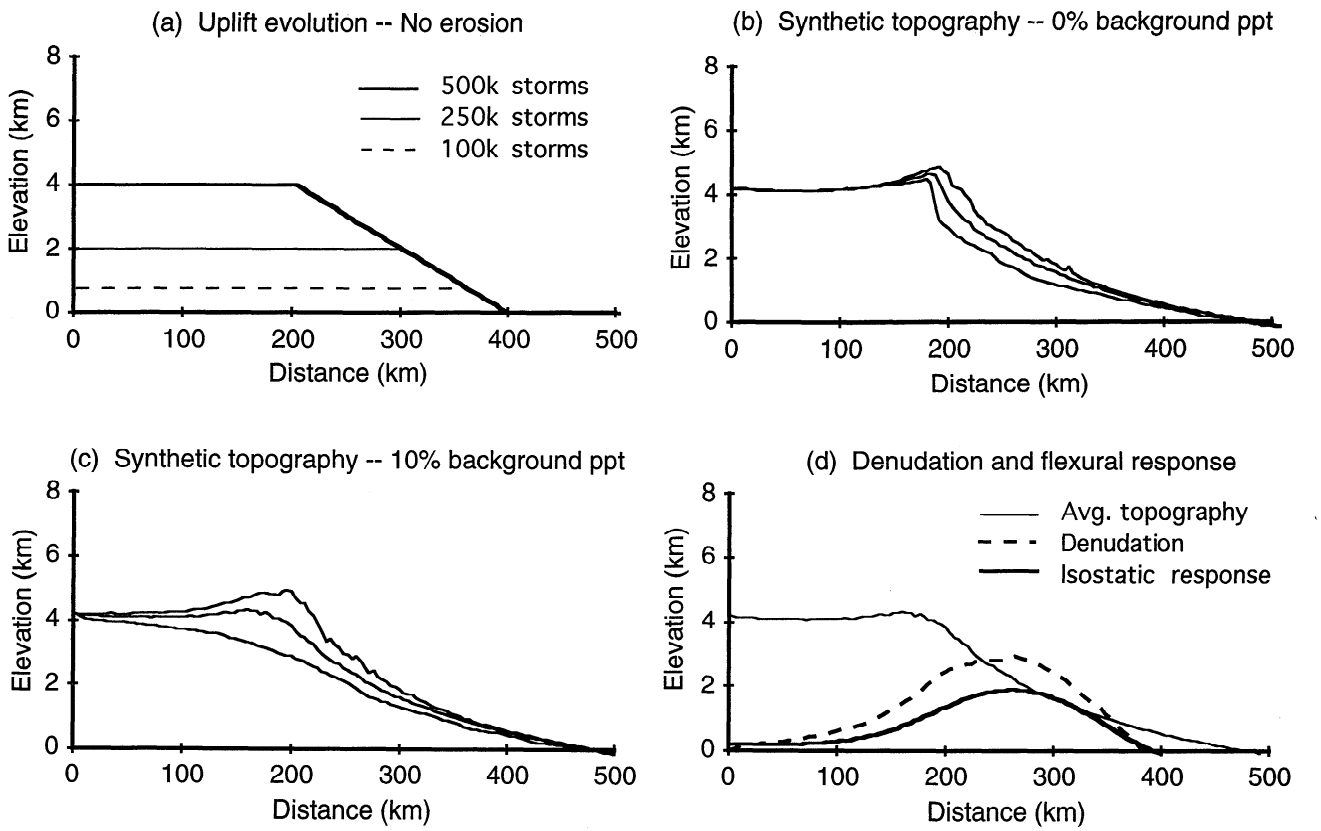

Figure 11. Results from the erosional modeling shown as profiles perpendicular to strike. (a) Profiles showing the evolution of the uplift pattern in the absence of any erosion. Temporal scaling is with respect to the number of (nonerosive, in this case) storm events (in thousands). (b) Maximum, average, and minimum topographic profiles at 750,000 storm events showing the result of purely orographic precipitation and associated erosion applied to the tectonic model given in Figure 11a. Uplift occurred during the first 500,000 storms. (c) Same as Figure 11b, but with the addition of 10% uniform background precipitation in addition to orographic precipitation. (d) Average topographic profile from Figure 11c superposed with curves showing profiles of denudation and the isostatic response to the denudation.

condition for all simulations was a tilted plane (200 m total relief) with a preexisting, mature drainage network. Tectonic uplift occurred simultaneously with erosion for the first 500,000 storms of each simulation, after which erosion occurred without uplift.

The coupled orographic-erosional system tends to produce a steep slope (Figure 11b). Since both the orographic and erosional laws are, to a first approximation, slope-dependent, their coupling produces a positive feedback that preferentially removes material from the lower slopes of the topography, resulting in the observed steepening. As erosion progresses the plateau margin retreats while preserving the steep slope, similar in form to the retreat of long-wavelength escarpments observed at passive margins [e.g., *Stüwe*, 1991].

In the model, nothing exists to limit the steepening of the mountain front, and the feedback between erosion and precipitation tends to be strong enough to preclude external drainage, seen as the upwarp of the minimum topographic envelope at the plateau edge in Figure 11b. The addition of a small amount of nonorographic background precipitation (10% of the orographic peak) preserves the external drainage (Figure 11c). Although both the Tibetan plateau and the Altiplano plateau are internally drained, the drainage divides occur well within the plateau interiors, and the Eastern Cordillera and Himalayan margins are both externally drained. Accordingly, Figure 11c represents a more appropriate simulation of the Beni and Himalayan fronts.

Up to 4 km of denudation have occurred along the plateau front during the simulation shown in Figure 11c, and regional isostatic uplift occurs in response to this erosion (Figure 11d). As the regional slope steepens, the taper of the topography becomes significantly shorter than the flexural wavelength, and a flexural lip is formed at the margin of the plateau (Figure 11c). An additional component of this marginal uplift is generated by canyon incision across the plateau margin, which also tends to increase the altitude of the peaks [*Wager*, 1937; *Molnar and England*, 1990; *Burbank*, 1992]. The magnitude and wavelength of the marginal uplift are highly dependent on the low flexural rigidity. Rigidities appropriate for the foreland region (e.g., 10^{24} N m) yield broad, low-amplitude peaks rather than the narrow, higher peaks shown here.

The topographic evolution predicted by the model differs from that predicted by a simple height dependent erosion law or simple diffusional law. Both of these laws would predict a steady lowering of regional slope through time and a reduction in the magnitude of the topographic lip at the plateau margin. Furthermore, neither law would be able to generate

topographic relief when applied to a three dimensional surface [*Newman and Turcotte*, 1992].

It should be noted that the model does have several deficiencies. The coupling between the orography and topography is so strong that getting moisture to the highest peaks without adding background precipitation is problematic. In reality, pulsed moisture release from glacial/interglacial cycles may aid the erosion of the highest peaks [*Isacks*, 1992]. In addition, the erosion model does not generally produce fractal scaling of topography without the use of a diffusion algorithm to damp the higher frequencies. This conflicts with the observation that topography is fractal over those length scales where fluvial processes are most efficient [*Montgomery and Dietrich*, 1992].

Synthesis and Discussion

Topographic Evolution

We have presented observations suggesting that erosion is a more significant geomorphic agent in the Beni region of Bolivia and the central Himalaya than in southern Bolivia, and we have presented a numerical model to explain major features of the long-wavelength topography that characterize the high erosion regions. We conclude that orographic precipitation arising from saturated air impinging on a plateau margin will tend to drop moisture low on the slope. This orographic focusing, coupled with any sort of slope-dependent erosion, will tend to steepen and eat back the plateau margin (Figure 12). Neither erosion rate nor precipitation can be regarded as simple functions proportional to height. We also note that simple diffusional models for landform evolution would predict a steady lowering of regional slope through time, not the escarpment retreat deduced for the central Andes and Himalaya.

In the model, the isostatic response to removing mass and steepening the topography generates peaks in the maximum topographic envelope at the plateau edge, analogous to the observed high topography of the high Himalaya and Eastern Cordillera (Figure 12). In fact, in the Bolivian Andes there is a correlation between the height of the maximum topographic envelope at the plateau margin and the regional precipitation. South of ~18°S, in areas with relatively low precipitation and denudation rates, no lip of extreme topography is present at the plateau margin. North of 18°S, in regions with higher precipitation and denudation, the peaks of the Cordillera Real rise 2 km above the average elevation of the Eastern Cordillera and 3 km above the average elevation of the Altiplano plateau [*Isacks*, 1988]. Nevertheless, this isostatic uplift may be combined with other aspects of the tectonics occurring at the plateau margins. The high topography at the margins may also a remnant of localized Miocene thrusting (e.g., the MCT, Eastern Cordillera system), and there is a clear association between the highest topography and lithology, indicating that differential erodiblity plays a major role in defining the topographic peaks once the rock uplift has taken place.

The isostatic effects of eroding the MCT overthrust may also have interesting implications for the present structural geometry of the Himalaya. In particular, a bend in the main décollement under the high Himalyan peaks, derived from well logs, seismicity, and seismic reflection profiling [*Ni and Barazangi*, 1984; *Zhao and Nelson, 1993*], appears to match the bend in the Moho deduced from gravity modeling (Figure

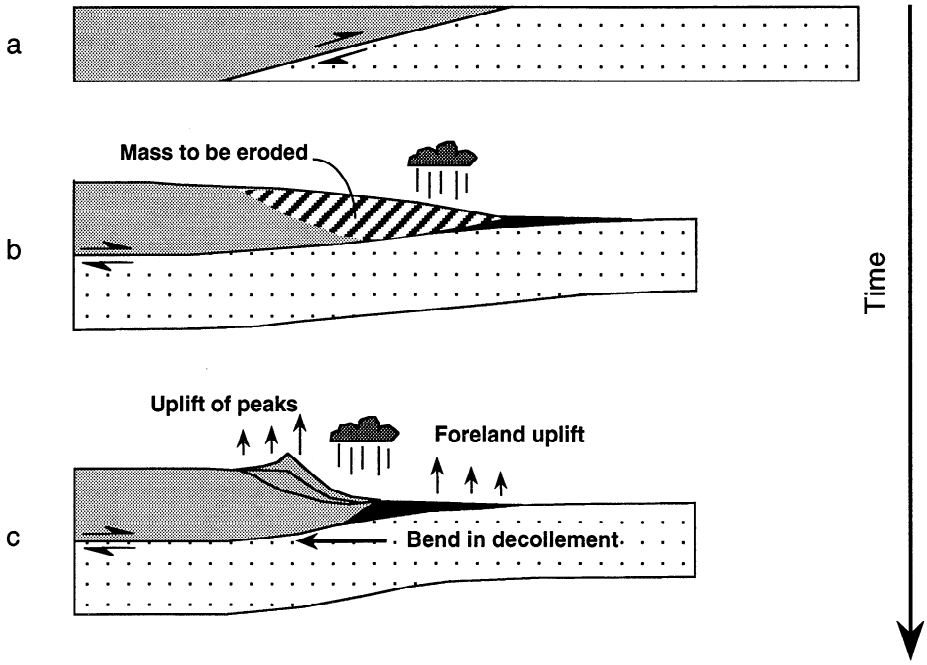

Figure 12. Cartoon (not to scale) illustrating the major interactions discussed in this study. Crustal scale thrusting (e.g., the MCT) produces original tectonic topography (Figures 12a and 12b). Orographic precipitation and erosion causes a certain amount of mass to be removed from the front of the thrust sheet (hatched area in Figure 12b). Through time, the topographic front steepens and retreats (Figure 12c), and erosional relief is generated at the margin (symbolized by maximum, average, and minimum curves shown). Isostatic rebound from this erosion causes uplift of the peaks, uplift within the foreland, and migration of the main décollement, as discussed in the text. No attempt has been made to show younger deformation within the foreland. The mass influx from that deformation would tend to counteract the erosional isostatic rebound within the foreland.

6b) [*Lyon-Caen and Molnar*, 1983, 1985; *Molnar*, 1984]. *Molnar* [1987] and *Ni and Barazangi* [1984] suggested that the high topography of the Himalayan peaks may reflect movement on the MCT/MBT system, with constant slip on the décollement placing the highest vertical particle velocities over the bend, thus creating the highest Himalayan topography.

Alternatively, we speculate that the observed bend in the décollement could be simply a passive flexural response to the edge of the plateau. Where the topography is high, the Indian plate must be deflected more due to greater loading [e.g., *Lyon-Caen and Molnar*, 1983]. As erosion continues, and the plateau margin continues to erode toward the north, the décollement under the Lesser Himalaya must be isostatically uplifted, translating the bend toward the north (Figure 12). Although the bend in the decollement should correlate with the position of the high Himalayan peaks, the high peaks may not be a consequence of the bend.

Implications for Mass Flux

The erosion and retreat of the Beni and Himalayan fronts represent a considerable efflux of mass from the tectonic wedges. This leads to a fundamental question: Are the Andean and Himalayan tectonic wedges currently gaining or losing mass? In other words, is thin-skinned deformation within the foreland presently keeping pace with the erosion of the older thrust sheets?

Simple mass budget calculations, based on minimum denudation estimates and maximum shortening estimates, suggest that late Neogene denudation of the Himalaya may have outpaced the tectonic influx. In the Himalayan case, the balanced cross section presented by *Schelling* [1992] indicates that a minimum of 2000-3000 km^2 of cross-sectional area has been denuded from the MCT overthrust and Lesser Himalaya since the emplacement of the Mahabharat synclinorium. The exact value depends on the reconstruction of the missing portion of the MCT overthrust. Assuming that the erosion of the MCT overthrust from the Lesser Himalaya postdated major movement on the MCT, the maximum mass influx would occur if all deformation within the Lesser and Sub-Himalaya began after the emplacement of the Mahabharat crystallines. This mass influx would be equal to the total Lesser and Sub-Himalayan shortening multiplied by the average thickness of material worked into the wedge. Shortening estimates for the MBT/Sub-Himalayan system range from about 60 to 150 km [*Schelling*, 1992; *Molnar*, 1984]. Assuming that an average thickness of ~10 km has been offscraped from the Indian Shield to form the Lesser and Sub-Himalaya, the mass influx has been in the range of 600-1500 km^2.

These estimates indicate that the mass influx into the Himalayan wedge may not have kept pace with the erosion of the MCT overthrust. *Burbank* [1992] noted that the course of the Ganges river within the foreland basin stepped toward the Indian shield during the Plio-Pleistocene and suggested that increased erosional unloading in the Himalaya isostatically upwarped the proximal foreland during this time. The mass deficit calculated here could account for the unloading.

In contrast, the cross section of *Roeder* [1988], the fission track data of *Benjamin* [1986], and sediment volumes within the Amazon fan [*Damuth and Flood*, 1984; *Kumar*, 1978] suggest that about 500-1000 km^2 of cross-sectional area has been denuded from the Beni front in Bolivia in the past 10-15 m.y. Shortening estimates for the Subandean belt range from 80 to 150 km, with deformation initiating within the past 10 m.y. [*Roeder*, 1988; *Gubbels et al.*, 1993]. Assuming that an average of ~6-8 km of Phanerizoic cover has been worked into the Subandean belt (Roeder, 1988), the total mass influx amounts to about 500-1200 km^2. This suggests an approximate mass balance since the initiation of Subandean deformation. These conclusions assume that the shortening estimates are accurate within the ranges given above; a factor of 2 increase or decrease in shortening could account for either surplus or deficit.

The difference in the sign of net mass flux in the Beni and Himalayan regions reflects a difference in erosion rather than tectonics. The most recent mass influx due to thin-skinned deformation is similar in the two regions. Taking the amount of Subandean shortening as 120 km and taking the initiation of shortening at 5-10 Ma [*Gubbels et al.*, 1993], gives shortening rates of 1.2-2.4 cm/yr, similar to the 1.0-2.5 cm/yr estimated for the Neogene convergence across the Himalaya [*Molnar*, 1984, 1987]. Nevertheless, the erosional efflux from the Himalaya during the last 5-15 m.y. appears to have been much greater than the equivalent erosion within the Eastern Cordillera.

When viewed over the timescale of the entire continental collision the Himalaya have tectonically advanced from the Indus-Tsangpo Suture and therefore have experienced a net increase in mass over this longer timescale. It follows that the trend toward net mass decrease within the Himalayan wedge must be a relatively recent phenomenon.

Two factors may account for the apparent change. First, the tectonic influx into the Himalayan wedge has probably decreased through time. During its period of activity the MCT must have sheared off the entire upper crust of India (~20-25 km thickness). In contrast, more recent deformation associated with the MBT within the lesser Himalaya and Sub-Himalaya has only involved the Phanerozoic cover of the Indian Shield or, most recently, only the Cenozoic foreland basin sediments (~ 5-10 km thickness). Assuming that underthrusting continued at approximately the same rate through time, this upward jump in décollement level implies that the rate at which Indian crust has been worked into the Himalayan wedge has decreased by at least a factor of 2 during the Neogene. Thus the hypothesized switch from mass surplus to mass deficit could have occurred even with a constant Neogene erosion rate.

A second factor may relate to late Cenozoic climate change and an associated increase in erosion rate in the Himalaya. Existing data suggest that the Indian monsoon may have initiated at ~8 Ma [*Kroon et al.*, 1991; *Prell and Kutzbach*, 1992]. The sudden influx of moisture arising from the monsoonal circulation could certainly have led to an acceleration of denudation at the plateau margin, as hypothesized by *Molnar and England* [1990]. In addition, alternating storage and release of moisture during Plio-Pleistocene glaciations within the high Himalaya may have led to increased erosion rates.

Conclusions

In this paper, we have shown that systematic along-strike variations in the topography of the eastern margin of the central Andean plateau can be correlated with along-strike variations in climate and Neogene erosion rate. Furthermore,

the physiography of the high precipitation Beni region of the central Andes has much in common with the physiography of the Nepal Himalayan front. As such, we argue that the Beni and Himalayan fronts represent cases where the topography is largely determined by the erosional/climatic regime, rather than by tectonics. A simple physical model suggests that high rates of orographic precipitation coupled with slope-dependent erosion can lead to the physiography that characterizes the Beni and Himalayan regions, with a steep frontal escarpment and high marginal peaks. As the erosional system continues to evolve, the topographic expression of the plateau margin may retreat toward the plateau interior in response to changes in tectonic mass influx or erosional mass efflux. Geologic evidence from the Bolivian Andes and Himalaya suggests that plateau margin has, in fact, retreated. In the case of the Himalaya, it is clear that this retreat has not been a steady process but that the MCT overthrust first advanced toward the foreland and subsequently retreated due to erosion.

Appendix: Description of Numerical Model

In this section we describe the sediment transport and orographic components of the numerical model for eroding mountain belts. Values for the parameters used in the modeling are summarized in Table 1.

Sediment Transport

A number of models have been published to describe erosion, transport, and deposition of sediment on a macroscale. Early attempts to couple tectonics and erosion used simple height-dependent erosion laws [e.g., *Dahlen and Suppe*, 1988]. Other authors have discussed sediment transport in terms of a diffusion equation, derived by assuming that sediment flux is proportional to stream power, and assuming either uniform water flux [*Culling* 1960; *Kenyon and Turcotte*, 1985; *Flemings and Jordan*, 1989] or spatially variable water flux [*Willgoose et al.*, 1991].

An alternative approach, used here, is to model sediment transport as an advective process, similar to that used by *Beaumont et al.* [1992] and *Stüve* [1991]. We use a modified version of GILBERT, a cellular-automata fluvial transport model developed by *Chase* [1992]. Random storm events ("precipitons"), treated here as units of water flux, are dropped on the topographic grid. The precipiton runs downhill, following the local gradient, and a potential erodibility E and carrying capacity C are calculated at each step on the grid. Both quantities are considered to be proportional to the local stream power:

Table 1. Model Parameters

Parameter	Value
Flexural rigidity D	5 x 10^{22} N m
Erosion parameters	
k_e	0.08
k_c	20.0
Lapse rate γ	6.7°C/km
Plateau uplift rate	80 m/10^4 storms
Grid size	128 x 128 cells
Grid scale	4 km/cell

$$C, E = k_c, k_e \left(q_w \frac{\partial h}{\partial x} \right) \tag{1}$$

where q_w is the magnitude of the water flux, $h(x,y)$ is the topography, and k_c and k_e are constants. If the carrying capacity exceeds the amount of material currently carried by the precipiton M, the precipiton will erode a certain amount of material from the topographic grid up to E but not exceeding C - M. Alternatively, if the carrying capacity falls below the amount of material currently carried, the precipiton will deposit the difference M - C. We include no diffusional term, as the scale of "diffusional" geomorphic process (e.g., soil creep, solifluction, etc) are too small to be of interest on the lengthscale and timescale considered here. As noted above, all surface mass transfer is compensated isostatically. At the boundaries of the grid, precipitons (and all mass they carry) are lost.

Orographic Precipitation

Although the driving forces behind the large-scale atmospheric circulations differ considerably between the Tibetan and Andean plateaus, the two precipitation fields can be described with a common physical model. In the case of Tibet, the large surface area of the plateau results in a widespread convective instability as the plateau is heated during the summer. The resulting monsoonal circulation brings moist air from the Indian subcontinent up the Himalayan slopes. There the air cools, moisture condenses, and rainfall ensues. In the case of the Andes, the monsoonal circulation may be driven by sensible heating of the South American continent or possibly by the Altiplano plateau itself [*Rao and Erdogan*, 1989; *Gutman and Schwerdtfeger*, 1965]. The north-south trending Andes form an obstacle to the low-level anticyclonic flow induced by the resultant low-level low pressure cell. Accordingly, the air is mechanically lifted up the eastern slopes, producing orographic precipitation. While the explanation for the lifting of air up the plateau margins may differ between the two regions, the net effect in both cases is the transport of moist air upslope.

We have used these observations to construct a simplified model for orographic precipitation. We assume an incoming airflow directed perpendicular to the mountain front, an assumption supported by inspection of seasonal circulation charts [*Virji*, 1981]. The incoming air column is considered to flow as a unit over the average topography of the plateau front and surface, such that there is no vertical variation of air velocity. The incoming air column is broken into parcels of thickness dz, and each parcel is assigned a relative humidity $U(z)$. For the results presented here, $U(z)$ has been taken as 1.0, the condition for a saturated air column. Assuming a psuedo-adiabatic lapse rate (6.7°C/km), the temperature of each parcel may be calculated as it passes over the topography. From the Clausius-Clapeyron equation for condensation, the change in saturation vapor pressure of an air mass e_s as a function of change in temperature T may be written as

$$\frac{de_s}{dT} = \frac{Le_s}{R_v T^2} \tag{2}$$

where L represents the latent heat of condensation and R_v represents the gas constant for water vapor [*Iribarne and Godson*, 1981]. Integrating (2) yields

$$e_s = \exp\left\{\ln(e_{s0}) - \frac{L}{R_v T_0} - \frac{L}{R_v T}\right\}. \quad (3)$$

Equation (3) gives the saturation vapor pressure of an air parcel as a function of temperature, assuming a reference (sea level) saturation vapor pressure and temperature of e_{so} and T_o, respectively. The actual vapor pressure of the air parcel may be calculated according to the equation of state for moist air:

$$e = R_v T / \alpha_v \quad (4)$$

where α_v represents the specific volume of water vapor in the parcel.

In the orographic model, both the saturation vapor pressure and the actual vapor pressure are recalculated as each parcel is stepped across the topography. If the actual vapor pressure exceeds the saturation vapor pressure, the difference is considered as an amount of precipitation falling on the topography below. We then smooth the synthetic precipitation field using a 10 grid point (40 km) averaging window to remove excessive dependence on the high-frequency component of the topography.

Actual volumes of water falling over a period of years cannot be calculated without knowing the moisture flux advected toward the topography, which in turn requires knowledge of an appropriate time-averaged wind velocity. Instead, the model precipitation field is normalized to the maximum amount on the grid, and this array is then used as a spatial probability field to select storm locations. These storms are the precipitons described above. Thus, while the orographic model cannot predict precipitation rates, it does predict the spatial distribution of precipitation.

Scaling

The vertical dimension of the modeled topography is physically scaled by vapor pressure relations (3) and (4) in conjunction with the assumed adiabatic lapse rate of 6.7°C/km. The horizontal dimensions of the model are scaled by the flexure equation, and the resultant flexural wavelength. Temporal scaling of the model is somewhat arbitrary. The scaling is accomplished empirically by fixing the rate of thrust movement as a function of number of storm events (10,000 storm events per uplift event), and using a ratio of k_e/k_c that yields realistically integrated drainage networks for all simulations.

Acknowledgments. We thank T.E. Jordan, A.L Bloom, M. Barazangi, R.W. Allmendinger, D. Whitman, and other members Cornell Andes/EOS Project for useful discussions and/or reviews. JGR reviewers M. Ellis, T. Lowery, and L. Sonder made constructive comments that substantially improved the manuscript. We thank C.G. Chase for providing a copy of the landsculpting algorithm GILBERT for use in the modeling. The Asian digital topography was acquired through DARPA contracts F19628-88-K-0035 and F29601-91-DB08. This research was supported by NASA Graduate Student Researchers Program fellowships and NASA Earth Observing System Interdisciplinary contract NAGW-2638. INSTOC contribution 199.

References

Adams, J., Contemporary uplift and erosion of the Southern Alps, New Zealand, *Geol. Soc. Am. Bull., Part II, 91*, 1-114, 1980.

Baby, P., G. Herail, R. Salinas, and T. Sempere, Geometry and kinematic evolution of passive roof duplexes deduced from cross section balancing: Example from the foreland thrust system of the southern Bolivian Subandean zone, *Tectonics, 11*, 523-536, 1992.

Beaumont, C., P. Fullsack, and J. Hamilton, Erosional control of active compressional orogens, in *Thrust Tectonics*, pp. 1-19, Chapman and Hall, London, 1992.

Benjamin, M.T., Fission track ages on some Bolivian plutonic rocks: Implications for the Tertiary uplift and erosion history of the Altiplano-Cordillera Real, M.S. thesis, Dartmouth Coll., Hanover, N.H., 1986.

Benjamin, M.T., N. M. Johnson, and C. W. Naeser, Recent rapid uplift in the Bolivian Andes: Evidence from fission-track dating, *Geology, 15*, 680-683, 1987.

Burbank, D., Causes of recent Himalayan uplift deduced from deposited patterns in the Ganges Basin, *Nature, 357*, 680-683, 1992.

Burchfiel, B.C., Chen Z., K.V. Hodges, Liu Y., L.H. Royden, Deng C., and Xu J., The south Tibetan detachment system, Himalayan orogen: Extension contemporaneous with and parallel to shortening in a collisional mountain belt, *Spec. Pap.Geol. Soc. Am., 269*, 41 pp., 1992.

Chase, C.G., Fluvial landsculpting and the fractal dimesion of topography *Geomorphology, 5*, 39-57, 1992.

Culling, W.E.H., Analytical theory of erosion, *J. Geol., 68*, 336-344, 1960.

Dahlen, F.A., and J. Suppe, Mechanics, growth, and erosion of mountain belts, in Processes in Continental Lithospheric Deformation, *Spec. Pap. Geol. Soc. Am., 218*, 161-178, 1988.

Damuth, J.E., and R.D. Flood, Morphology, sedimentation processes, and growth pattern of the Amazon deep-sea fan, *Geo Mar. Lett., 3*, 109-117, 1984.

de Paor, D., and D. J. Anastasio, The Spanish external Sierra: A case history of the advance and retreat of mountains, *Natl. Geogr. Res., 3*, 199-209, 1987.

Dewey, J.F., R.M. Shackleton, Chang C., and Sun Y., The tectonic evolution of the Tibetan Plateau, *Philos. Trans. R. Soc. London, Ser. A, 327*, 379-413, 1988.

Evernden, J.F., S.J. Kriz, and M.C. Cherroni, Potassium-argon ages of some Bolivian rocks, *Econ. Geol., 72*, 1042-1061, 1977.

Fielding, E.J., B.L. Isacks, M. Barazangi, and C. Duncan, How flat is Tibet?, *Geology, 22*, 163-167, 1994.

Flemings, P.B., and T.E. Jordan, A synthetic stratigraphic model of foreland basin development, *J. Geophys. Res., 94*, 3851-3866. 1989.

Francis, P.W., M.C.W. Baker, and C. Halls, The Kari-Kari caldera, Bolivia, and the Cerros Rico stock, *J. Volcanol. Geotherm. Res., 10*, 113-124, 1981.

Gansser, A., *Geology of the Himalayas*, 289 pp., Wiley-Interscience, New York, 1964.

Grant, J.N., C. Halls, W.A. Salinas, and N.J. Snelling, K-Ar ages of igneous rocks and mineralization in part of the Bolivian tin belt: *Econ. Geol., 74*, 838-851, 1979.

Gubbels, T.L., Tectonics and geomorphology of the eastern flank of the Central Andes, 18° to 23° south latitude, Ph.D. thesis, 211 pp., Cornell Univ., Ithaca, N.Y., 1993.

Gubbels, T.L., B.L. Isacks, and E. Farrar, High-level surfaces, plateau uplift, and foreland development, Bolivian Central Andes, *Geology, 21*, 695-698, 1993.

Gutman, G.J., and W. Schwerdtfeger, The role of latent and sensible heat for the development of a high pressure system over the subtropical Andes, in the summer, *Meteorol. Rundsch., 18*, 69-75, 1965.

Guyot, J.L., J. Bourges, R. Hoorelbecke, M.A. Roche, H. Calle, J. Cortes, and M.C.B. Guzman, Exportation de matieres en suspension des Andes vers l'Amazonie par le Rio Beni, Bolivie, in Sediment Budgets – Proceedings of the Porto Alegre Symposium, December 1988, *IAHS Publ. 174*, 443-451, 1988.

Guyot, J.L., H. Calle, J. Cortes, and M. Pericra, Transport de matieres dissoutes et particulaires des Andes vers le Rio de La Plata par les tributaires boliiviens (rios Pilcomayo et Bermejo) du Rio Paraguay, *Hydrol. Sci. J., 35*, 653-665, 1990.

Harrison, T.M., P. Copeland, W.S.F. Kidd, and Yin, A., Raising Tibet, *Science, 255*, 1663-1670, 1992.

Hastenrath, S., *Climate Dynamics of the Tropics*, 488 pp., Kluwer Academic, Norwell, Mass., 1991.

Hoffmann, A.J. (Ed.), *Climatic Atlas of South America*, World Meterological Organization, UNESCO, Geneva, 1979.

Hubbard, M., L. Royden, and K. Hodges, Constraints on unroofing rates in the high Himalaya, eastern Nepal, *Tectonics, 10*, 287-298, 1991.

Iribarne, J.V., and W.L. Godson, *Atmospheric Thermodynamics*, 259 pp., D. Reidel, Norwell, Mass., 1981.

Isacks, B.L., Uplift of the central Andean plateau and bending of the Bolivian orocline, *J. Geophys. Res., 93*, 3211-3231, 1988.

Isacks, B.L., 'Long-term' land surface processes: Erosion, tectonics and climate history in mountain belts, in *Terra-1: Understanding the Terrestrial Environment*, edited by P.M. Mather, pp. 21-36, Taylor and Francis, London, 1992.

Kenyon, P.M., and D.L. Turcotte, Morphology of a delta prograding by bulk sediment transport, *Geol. Soc. Am. Bull., 96*, 1457-1465, 1985.

Kooi, H., and C. Beaumont, Escarpment evolution of high-elevation rifted margins: Insights derived from a surface processes model that combines diffusion, advection, and reaction, *J. Geophys. Res.*, this issue.

Koons, P.O., The topographic evolution of collisional mountain belts: A numerical look at the Southern Alps, New Zealand, *Am. J. Sci., 289*, 1041-1069, 1989.

Koons, P.O., Two-sided orogen: Collision and erosion from the sandbox to the Southern Alps, New Zealand, *Geology, 18*, 679-682, 1990.

Korzoun, V.I. (Ed.), *Atlas of World Water Balance*, UNESCO Press, Paris, 1977.

Kroon, D., T. Steens, and S.R. Troelstra, Onset of monsoonal related upwelling in the western Arabian Sea as revealed by planktonic foramifers, *Proc. Ocean Drill. Program, Sci. Results, 117*, 257-263, 1991.

Kumar, N., Sediment distribution in the western Atlantic off northern Brazil – Structural controls and evolution, *AAPG Bull., 62*, 273-294, 1978.

Le Pinchon, X., M. Fournier, and L. Jolivet, Kinematics, topography, shortening, and extrusion in the India-Eurasia collision, *Tectonics, 11*, 1085-1098, 1992.

Lyon-Caen, H., and P. Molnar, Constraints on the structure of the Himalaya from gravity anomalies and a flexural model of the lithosphere, *J. Geophys. Res., 88*, 8171-8191, 1983.

Lyon-Caen, H., and P. Molnar, Gravity anomalies, flexure of the Indian plate, and structure, support, and evolution of the Himalaya and Ganga Basin, *Tectonics, 4*, 513-538, 1985.

Lyon-Caen, H., P. Molnar, and G. Suarez, Gravity anomalies and flexure of the Brazilian Shield beneath the Bolivian Andes, *Earth Planet. Sci. Lett., 75*, 81-92, 1985.

Macfarlane, A.M., K.V. Hodges, and D. Lux, A structural analysis of the Main Central Thrust zone, Langtang National Park, central Nepal Himalaya, *Geol. Soc. Am. Bull., 104*, 1389-1402, 1992.

McBride, S.L., R.C.R. Robertson, A.H. Clark, and E. Farrar, Magmatic and metallogenetic episodes in the northern tin belt, Cordillera Real, Bolivia, *Geol. Rundsch., 72*, 685-713, 1983.

McBride, S.L., A.H. Clark, E. Farrar, and D.A. Archibald, Delimitation of a cryptic Eocene tectono-thermal domain in the Eastern Cordillera of the Bolivian Andes through K-Ar dating and ^{40}Ar-^{39}Ar step-heating, *J. Geol. Soc. London, 144*, 243-255, 1987.

Molnar, P., Structure and tectonics of the Himalaya: Constraints and implications of geophysical data, *Annu. Rev. Earth Planet. Sci., 12*, 489-518, 1984.

Molnar, P., Inversion of profiles of uplift rates for the geometry of dip-slip faults at depth, with examples from the Alps and the Himalaya, *Ann. Geophys., Ser. B, 5*, 663-670, 1987.

Molnar, P., and P. England, Late Cenozoic uplift of mountain ranges and global climatic change: Chicken or egg?, *Nature, 346*, 29-34, 1990.

Montgomery, D.R., and W.E. Dietrich, Channel initiation and the problem of landscape scale, *Science, 255*, 826-830, 1992.

Newman, W.I., and D.L. Turcotte, Cascade model for fluvial geomorphology, *Geophys. J. Int., 100*, 433-439, 1990.

Ni, J., and M. Barazangi, Seismotectonics of the Himalayan collision zone: Geometry of the Underthrusting Indian Plate Beneath the Himalaya, *J. Geophys. Res., 89*, 1147-1163, 1984.

Pareja, J., C. Vargas, R. Suarez, R. Ballon, R. Carrasco, and C. Villaroel, Mapa geologico de Bolivia y memoria explicativa, scale 1:1,000,000, 2 sheets, Yacimentos Petroliferos Fiscales Bolivianos y Servi. Geol. de Bolivia, La Paz, Bolivia, 1978.

Prell, W.L., and J.E. Kutzbach, Sensitivity of the Indian monsoon to forcing parameters and implications for its evolution, *Nature, 360*, 647-652, 1992.

Rao, G.V., and S. Erdogan, The atmospheric heat source over the Bolivian plateau for a mean January, *Boundary Layer Meterol., 46*, 13-33, 1989.

Roeder, D., Andean-age structure of Eastern Cordillera (Province of La Paz, Bolivia), *Tectonics, 7*, 23-39, 1988.

Schelling, D., The tectonostratigraphy and structure of the eastern Nepal Himalaya, *Tectonics, 11*, 925-943, 1992.

Sempere, T., G. Herail, J. Oller, and M.G. Bonhomme, Late Oligocene-early Miocene major tectonic crisis and related basins in Bolivia, *Geology, 18*, 946-949, 1990.

Steinhauser, F. (Ed.), *Climatic Atlas of North and Central America*, World Meteorological Organization, UNESCO, Geneva, 1979.

Stocklin, J., Geology of Nepal and its regional frame, *J. Geol. Soc. London, 137*, 1-34, 1980.

Strahler, A.N., Hypsometric (area-altitude curve) analysis of erosional topography, *Geol. Soc. Am. Bull., 63*, 1117-1141, 1952.

Stüwe, K., Flexural constraints on the denudation of assymetric mountain belts, *J. Geophys. Res., 96*, 10,401-10,408, 1991.

Suppe, J., Mechanics of mountain building and metamorphism in Taiwan, *Mem. Geol. Soc. China, 4*, 67-89, 1981.

Suppe, J., *Principles of Structural Geology*, 537pp., Prentice-Hall, Englewood Cliffs, N.J., 1985.

Tucker, G.E., and R.L. Slingerland, Erosional dynamics, flexural isostasy, and long-lived escarpments: A numerical modeling study, *J. Geophys. Res.*, this issue.

Turcotte, D.L., *Fractals and Chaos in Geology and Geophysics*, 221 pp., Cambridge University Press, New York, 1992.

Turcotte, D.L., and G. Schubert, *Geodynamics*, 450 pp., John Wiley, New York, 1982.

Virji, H., A preliminary study of summertime tropospheric circulation patterns over South America estimated from cloud winds, *Mon. Weather Rev., 109*, 599-610, 1981.

Wager, L.R., The Arun River drainage pattern and the rise of the Himalaya, *Geog. J., 89*, 239-250, 1937.

Willgoose, G., R.L. Bras, and I. Rodriguez-Iturbe, A coupled channel network growth and hillslope evolution model, 1, theory, *Water Resour. Res., 27*, 1671-1684, 1991.

Zhao, W. L., and W.J. Morgan, Uplift of Tibetan Plateau, *Tectonics, 4*, 359-369, 1985.

Zhao, W., and K.D. Nelson, Deep seismic reflection evidence for continental underthrusting beneath southern Tibet, *Nature, 366*, 557-559, 1993.

E.J. Fielding, T.L. Gubbels, B.L. Isacks, and J.G. Masek, INSTOC, Cornell University, Snell Hall, Ithaca, NY 14853-1504. (e-mail: Internet: masek@geology.cornell.edu)

(Received April 30, 1993; revised January 31, 1994;
accepted February 14, 1994.)